Inorganic Chemistry

Article

pubs.acs.org/IC

Low-Dimensional Porous Coordination Polymers Based on 1,2-Bis(4-pyridyl)hydrazine: From Structure Diversity to Ultrahigh CO_2/CH_4 Selectivity

Xiao-Min Liu, Rui-Biao Lin, Jie-Peng Zhang,* and Xiao-Ming Chen*

MOE Key Laboratory of Bioinorganic and Synthetic Chemistry, State Key Laboratory of Optoelectronic Materials and Technologies, School of Chemistry and Chemical Engineering, Sun Yat-Sen University, Guangzhou 510275, China

Supporting Information

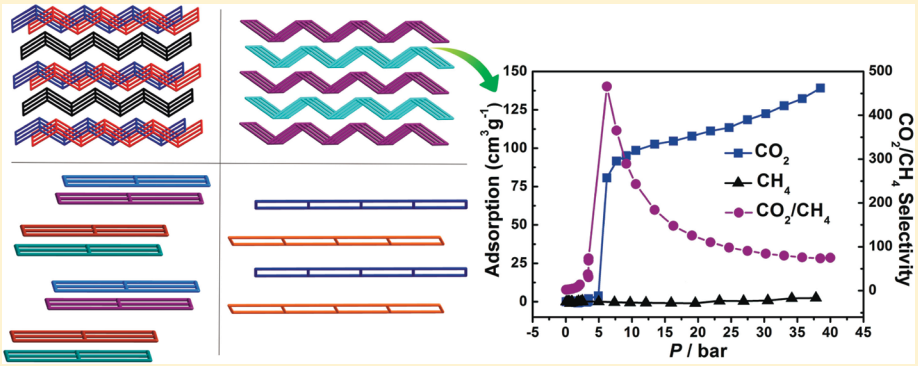

ABSTRACT: Solvothermal reactions of metal salts, benzenedicarboxylic acids, and 4,4′-azopyridine (azpy) in different conditions produced four coordination polymers, namely, $[Zn_3(bdc)_3(bphy)_3]\cdot 2DMF\cdot 10H_2O$ (**3**; H_2bdc = 1,4-benzenedicarboxylic acid, bphy = 1,2-bis(4-pyridyl)hydrazine, and DMF = *N*,*N*-dimethylformamide), $[Ni(bdc)(bphy)]\cdot DMF\cdot 3.5H_2O$ (**4**), $[Zn(nipa)(bphy)]\cdot EtOH$ (**5**; H_2nipa = 5-nitroisophthalic acid), and $[CoBr(bdc)_{0.5}(bphy)]\cdot 2DMA\cdot H_2O$ (**6**; DMA = *N*,*N*-dimethylacetamide), in which the azpy ligand was in situ reduced. Structural determination reveals that **3**−**5** consist of the same metal/ligand ratio and similar coordination modes, as well as similar two-dimensional square-grid networks, but differ from their packing/interpenetration modes. **3** consists of alternately arranged single layers and interweaved double layers. Single layers in **4** directly stack in an offset fashion, while **5** is constructed of interdigitated double layers. **6** is a one-dimensional ladderlike structure, which could be regarded as that half of the bridging benzenedicarboxylate ligands in **3**−**5** are replaced by monodentate bromide ions. Interestingly, the crystal structures of these low-dimensional coordination polymers contain considerable solvent-accessible voids. Thermogravimetric curves, powder X-ray diffraction, and gas sorption experiments were used to study the potential porosity of these structures, which indicated that they can all reversibly desorb and adsorb solvent molecules. In particular, **4** showed gated sorption behavior and high CO_2/CH_4 selectivity because of its flexible structure.

INTRODUCTION

Porous coordination polymers (PCPs) have attracted great attention in recent years for their intriguing architectures and potential applications as functional materials in catalysis, magnetism, nonlinear optics, gas storage, separation, etc.[1−7] To generate porosity, three-dimensional (3D) frameworks have been largely studied because high-dimensional structures usually possess stronger 3D framework rigidity, which facilitates the retention of pores after removal of the template molecules.[8−13] In contrast, the 3D supramolecular structures of low-dimensional frameworks sustained by weak interactions such as hydrogen-bonding, $\pi-\pi$-stacking, and van der Waals interactions generally collapse when the template guests are removed.[14,15] On the other hand, low-dimensional structural motifs can produce packing and/or structure diversity easier during crystallization, which has been a research interest in crystal engineering.[16−18] Also, they usually show structural changes in packing modes during guest adsorption/desorption, which is the base of flexible PCPs.[19,20] It has been shown that flexible PCPs are especially useful for selective sorption and separation applications.[21−24] Nevertheless, it is still a great challenge to control the dynamic nature of a crystalline coordination network, which can be brittle, flexible, or rigid.[25,26]

Theoretically, flexible PCPs could be obtained by means of a flexible ligand, framework entanglement, weak interaction between multiple frameworks, etc.[27−30] In practice, choosing or designing a suitable ligand is the most important strategy in constructing the coordination network with targeted structures and properties. Recently, we found that 4,4′-azopyridine (azpy)

Received: January 14, 2012
Published: May 7, 2012

   dx.doi.org/10.1021/ic300097y | *Inorg. Chem.* 2012, 51, 5686−5692

Table 1. Crystal Data and Structure Refinement for Compounds 3−6

	3	4	5	6
formula	$C_{60}H_{76}N_{14}O_{24}Zn_3$	$C_{21}H_{28}N_5O_{8.5}Ni$	$C_{20}H_{19}N_5O_7Zn$	$C_{22}H_{32}N_6O_5BrCo$
fw	1573.55	545.17	506.80	599.36
space group	$P2/c$	$P2_1/n$	$P2_1/n$	$P2_1/n$
a/Å	10.9425(13)	10.0803(11)	10.1848(10)	14.1464(16)
b/Å	21.354(2)	15.8190(18)	11.1036(11)	10.7476(12)
c/Å	18.840(2)	16.3208(18)	19.1820(18)	18.141(2)
β/deg	105.218(2)	101.034(3)	94.397(2)	97.938(2)
V/Å^3	4247.8(9)	2554.4(5)	2162.9(4)	2731.7(5)
Z	2	4	4	4
D_c/g cm^{-3}	0.975	1.064	1.415	0.990
μ/mm^{-1}	0.888	0.782	1.178	2.097
GOF	1.003	1.002	1.006	1.002
R1[a] [$I > 2\sigma(I)$]	0.0480	0.0593	0.0405	0.0532
wR2[b] (all data)	0.1387	0.1090	0.1077	0.1601

[a] $R1 = \sum||F_o| - |F_c||/\sum|F_o|$. [b] $wR2 = [\sum w(F_o^2 - F_c^2)^2/\sum w(F_o^2)^2]^{1/2}$.

could be in situ reduced into 1,2-bis(4-pyridyl)hydrazine (bphy) during a solvothermal reaction.[31] The new bphy ligand is advantageous for constructing flexible networks. On the one hand, bphy possesses backbone flexibility arising from the long C−N−N−C single bonds. On the other hand, the hydrazo group (−NH−NH−) moiety can serve as hydrogen-bonding sites for internetwork interactions and/or guest molecules. For example, we have synthesized two new 3D PCPs, [Zn(bdc)(bphy)] (**1**) and [Zn(bdc)(bphy)$_{0.5}$] (**2**), with uninodal 4-connected **dmp** and **pcu** topologies, by reacting $Zn(NO_3)_2$, 1,4-benzenedicarboxylic acid (H_2bdc), and azpy with corresponding metal/ligand molar ratios in *N*,*N*-dimethylformamide (DMF)/*N*,*N*-dimethylacetamide (DMA)/ethanol (EtOH) at 160 °C, both of which demonstrate dramatic framework flexibility upon inclusion of different solvent molecules.[31] For example, **1** was synthesized as two guest-induced framework-distortional isomers, [Zn(bdc)(bphy)]·DMF·H_2O (**1a**) and [Zn(bdc)(bphy)]·EtOH·H_2O (**1b**), by using DMF and EtOH as solvents, respectively.

In this work, we further investigated the application of this new solvothermal in situ ligand reaction in the construction of new coordination flexible PCPs by varying the reaction conditions and/or using other aromatic acids as the coligands. Four new low-dimensional coordination polymers showing interesting structures and gas sorption properties have been successfully synthesized and characterized.

EXPERIMENTAL SECTION

Materials and General Methods. Commercially available reagents were used as received without further purification. The ligand azpy was prepared according to a reported method.[32] Electrospray ionization mass spectrometry (ESI-MS) spectra were measured on a Shimadzu LCMS-2010A apparatus using an ESI source with methanol as the mobile phase. IR spectra were recorded with a Bruker TENSOR 27 Fourier transform infrared spectrophotometer on KBr pellets in the range of 4000−400 cm^{-1}. Elemental analyses (C, H, and N) were performed on a Perkin-Elmer 240 elemental analyzer. Thermogravimetric (TG) analyses were performed on a Netzsch TG 209 instrument in flowing N_2 with a heating rate of 10 °C min^{-1}. Powder X-ray diffraction (PXRD) measurements were performed on a Bruker D8 ADVANCE X-ray diffractometer with Cu Kα radiation. For variable-temperature (VT)PXRD measurements, the diffraction patterns at different temperatures were recorded after the sample had stayed at the respective temperature for 30 min in a N_2 atmosphere. CO_2 and CH_4 sorption measurements were performed with Belsorp-Max and Belsorp-HP automatic volumetric adsorption apparatuses.

*Syntheses of [Zn$_3$(bdc)$_3$(bphy)$_3$]·2DMF·10H$_2$O (**3**).* A mixture of $Zn(NO_3)_2·6H_2O$ (0.5 mmol, 148 mg), H_2bdc (1 mmol, 40 mg), and azpy (0.5 mmol, 58 mg) in 15 mL of DMF was stirred at 60 °C for 30 min, then sealed in a Teflon-lined autoclave, and heated to 160 °C for 2 days. After the autoclave was cooled to room temperature at 5 °C h^{-1}, the mother liquid was decanted, and the crystals were rinsed three times with DMF (8 mL × 3) and dried in air for 1 h (yield ∼80% based on Zn). Anal. Calcd for $C_{60}H_{76}N_{14}Zn_3O_{24}$: C, 45.80; H, 4.87; N, 12.46. Found: C, 45.71; H, 4.83; N, 12.41. IR (KBr, cm^{-1}): 3731 (w), 3627 (w), 2360 (s), 1623 (s), 1559 (m), 1480 (w), 1389 (s), 1104 (w), 1024 (w), 848 (m), 748 (s), 720 (s), 669 (m), 594 (w).

*[Ni(bdc)(bphy)]·DMF·3.5H$_2$O (**4**).* The synthesis of **4** was similar to that of **3** except that $Ni(NO_3)_2·6H_2O$ (0.5 mmol, 90 mg) was used instead of $Zn(NO_3)_2·6H_2O$ (yield ∼70% based on Ni). Anal. Calcd for $C_{21}H_{28}N_5O_{8.5}Ni$: C, 46.27; H, 5.18; N, 12.85. Found: C, 46.21; H, 5.12; N, 12.79. IR (KBr, cm^{-1}): 3284 (m), 2490 (w), 1668 (w), 1619 (s), 1541 (m), 1439 (w), 1402 (s), 1353 (w), 1305 (w), 1211 (m), 1057 (w), 1016 (s), 842 (m), 817 (m), 751 (m), 537 (m).

*[Zn(nipa)(bphy)]·EtOH (**5**).* A mixture of $Zn(NO_3)_2·6H_2O$ (0.5 mmol, 148 mg), H_2nipa (1 mmol, 40 mg), and azpy (0.5 mmol, 58 mg) in 15 mL of EtOH was stirred at 60 °C for 30 min, then sealed in a Teflon-lined autoclave, and heated to 160 °C for 2 days. After the autoclave was cooled to room temperature at 5 °C h^{-1}, the mother liquid was decanted, and the crystals were rinsed three times with EtOH (8 mL × 3) and dried in air for 0.5 h (yield ∼78% based on Zn). Anal. Calcd for $C_{20}H_{19}N_5O_7Zn$: C, 47.40; H, 3.78; N, 13.82. Found: C, 47.45; H, 3.71; N, 13.89. IR (KBr, cm^{-1}): 3236 (m), 2459 (w), 1681 (m), 1621 (s), 1569 (m), 1535 (w), 1496 (m), 1367 (s), 1344 (m), 1214 (s), 1058 (s), 824 (m), 731 (s), 659 (w), 612 (w), 527 (w).

*[CoBr(bdc)$_{0.5}$(bphy)]·2DMA·H$_2$O (**6**).* The synthesis of **6** was similar to that of **3** except that $CoBr_2$ (0.5 mmol, 108 mg) and DMA were used instead of $Zn(NO_3)_2·6H_2O$ and DMF (yield ∼50% based on Co). Anal. Calcd for $C_{22}H_{32}N_6O_5BrCo$: C, 44.09; H, 5.38; N, 14.02. Found: C, 44.12; H, 5.35; N, 14.09. IR (KBr, cm^{-1}): 3424 (w), 2360 (m), 1614 (s), 1501 (w), 1382 (s), 1207 (m), 1054 (w), 1019 (s), 827 (s), 748 (s), 589 (w).

X-ray Crystallography. Diffraction data were collected on a Bruker Apex CCD area-detector diffractometer with Mo Kα radiation at 93(2) K. The structures were solved by direct or Patterson methods and refined by the full-matrix least-squares method using *SHELXTL*. All H atoms were placed geometrically, and anisotropic thermal parameters were used to refine all non-H atoms of the frameworks. Most disordered guest molecules in **3**−**6** could not be modeled, and their electron density peaks were removed by the *SQUEEZE* route in *PLATON*. Their amounts were determined by TG results and

dx.doi.org/10.1021/ic300097y | Inorg. Chem. 2012, 51, 5686−5692

elemental analyses. The crystal data and structure refinement results are listed in Table 1.

RESULTS AND DISCUSSION

Synthesis. The azpy ligand was in situ reduced into bphy in the presence of metal salts and benzenedicarboxylic acids, giving rise to four new compounds, viz., **3**–**6**. It should be noted that the framework composition of **3** is identical with those of **1a**, **1b**, and **1** with the same **dmp** topology.[31] **1a** and **1b** were synthesized using different solvents, resulting in different guest inclusions and framework distortions, and they can be converted to the same guest-free phase **1** upon guest removal. Interestingly, the synthetic conditions, including the solvent, reactant, and reaction temperature, are basically identical for **1a** and **3**. The only difference is the pretreatment and reaction time of solvothermal syntheses. We found that stirring the suspension of starting materials at 60 °C before solvothermal treatment and shortening the reaction time was beneficial to producing **3**. Otherwise, the product would be **1a** or a mixture of **1a** and **3**. For reference, pure **1a** and **3** were synthesized at 160 °C for 3 and 2 days, respectively. These observations indicate that **1a** and **3** are thermodynamically and kinetically favored phases, respectively.

Crystal Structures. X-ray crystallographic analyses revealed that the N–N bond lengths [1.383(3)–1.399(7) Å] in **3**–**6** are obviously longer than the typical N=N bond lengths (e.g., 1.25 Å in azpy) yet similar to those of the N–N bonds (e.g., 1.36–1.44 Å in bphy). Besides, the absolute values of C–N–N–C torsion angles [73.9(2)–95.7(7)°] are distinctly deviated from the planar configuration of C–N=N–C moieties in azpy (180°) yet similar to that reported for free bphy [84.37(3)°]. All of these structural data confirm in situ reduction of the starting material azpy into bphy. There are two independent Zn^{2+} ions (Zn1 and Zn2), two bdc^{2-} ligands, and two bphy ligands in the asymmetric unit of **3**, although the coordination modes and/or molecular geometries of the two sets of metal ions/ligands are similar to each other. Each Zn^{2+} ion is four-coordinated with two carboxylate O atoms [Zn–O 1.923(3)–1.957(4) Å] from two bdc^{2-} ligands and two pyridyl N atoms [Zn–N 2.009(4)–2.025(4) Å] from two bphy ligands in a distorted tetrahedral geometry (Figure 1a,c). The bdc^{2-} ligands bridge two Zn^{2+} ions by two monodentate carboxylate groups, and the bphy ligands also link two Zn^{2+} ions by the two pyridyl ends. Consequently, the Zn ions are connected by bdc^{2-} and bphy into two sets of crystallographically independent two-dimensional (2D) wavy square-grid-like layers with the common **sql** topology (Figure 1b,d). Although the structures of these 2D networks are quite similar, their interpenetration modes are different. The networks containing Zn1 do not interpenetrate with each other, while those containing Zn2 undergo parallel 2-fold interpenetration to form double layers, with π–π-stacking interactions between the aromatic rings of bdc^{2-} from one layer and bdc^{2-} or bphy from another layer (Figures 1d and S3 in the Supporting Information). These double and single layers stack alternately to furnish the 3D structure of **3** (Figure 1e). The closest interactions between the double and single layers are the N–H···O hydrogen bonds between the hydrazo group of bphy and the carboxylate group of bdc^{2-} [N···O 2.794(3)–2.824(1) Å; N–H···O 160.4(2)–166.2(1)°] and π–π-stacking interactions between the pyridyl rings of bphy ligands (Figures S2 and S4 in the Supporting Information). The wavy square-grid structures and missing interpenetration in half of the packing layers in **3** result in a large solvent-accessible void of 45.6%, which is occupied by DMF and water molecules, as confirmed by TG and elemental analyses.[33] The hydrazo groups of bphy ligands not only form interlayer hydrogen bonds to sustain the 3D stacking structure but also behave as hydrogen-bonding donors to fix the guest water molecules [N–H···O 2.865(1) Å].

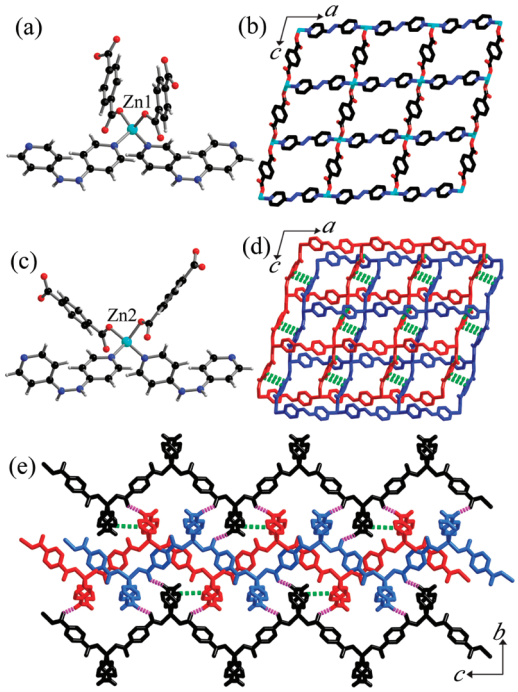

Figure 1. Perspective views of (a) the coordination environment of Zn1, (b) the corresponding single-layer coordination network, (c) the coordination environment of Zn2, (d) the corresponding parallel interpenetrated double-layer coordination network, and (e) the alternate stacking of the single and double layers in **3** (pink and green dotted lines represent hydrogen-bonding and π–π-stacking interactions, respectively).

Similar to **3**, **4** is also composed of square-grid-like coordination networks with **sql** topology. However, there is only one Ni^{2+} ion, one bdc^{2-} ligand, and one bphy ligand in the asymmetric unit. Being somewhat different from the Zn^{2+} ions in **3**, the Ni^{2+} ion is six-coordinated with four carboxylate O atoms [Ni–O 1.950(4)–2.195(7) Å] from two bdc^{2-} ligands and two N atoms [Ni–N 2.011(4)–2.052(4) Å] from two bphy ligands in distorted octahedral geometries (Figure 2a). In contrast to the complicated structure of **3**, the 2D **sql** networks are not interpenetrated in **4** (Figure 2b,c). These layers stack via interlayer N–H···O hydrogen-bonding [N···O 2.872(1) Å; N–H···O 158.2(2)°] and π–π-stacking interactions to form the 3D supramolecular structure (Figures S5 and S6 in the Supporting Information). By virtue of the wavy shapes of the layers and directional interlayer supramolecular interactions, there is a very small offset between adjacent layers, which is different from the staggered stacking fashion commonly observed for 2D layer structures (offset of adjacent layers is half of the grid size). Consequently, **4** also possesses large solvent-accessible voids of 44.1%, which is occupied by DMF and water molecules, forming hydrogen bonds with the hydrazo groups [N···O 2.794(3)–2.824(1) Å; N–H···O 110.1(2)–150.2(1)°].

Although the dicarboxylate $nipa^{2-}$ is bent, the local coordination configuration [Zn–O 1.950(4)–2.195(7) Å;

dx.doi.org/10.1021/ic300097y | Inorg. Chem. 2012, 51, 5686–5692

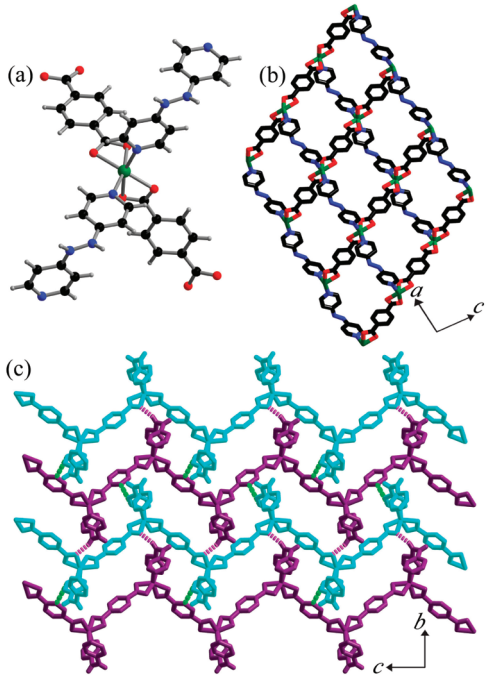

Figure 2. Perspective views of (a) the coordination environment of the Ni atom, (b) the 2D coordination network with **sql** topology, and (c) the stacking fashion of the 2D layers (pink and green dotted lines represent the interlayer hydrogen-bonding and $\pi-\pi$-stacking interactions, respectively) for **4**.

Zn−N 2.011(4)−2.052(4) Å] and the network topology in **5** are all similar to **3** constructed by the linear bdc^{2-} (Figure 3a,b). It is worth mentioning that the **sql** network of **5** is quite

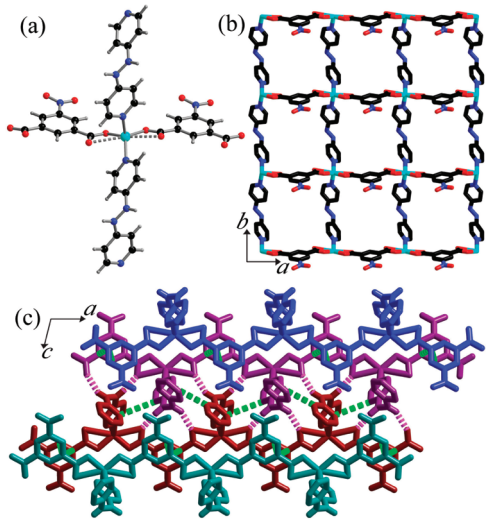

Figure 3. Perspective views of (a) the coordination environment of the Zn atom, (b) the 2D coordination network, and (c) the stacking of the 2D coordination layers (pink and green dotted lines represent the interlayer hydrogen-bonding and $\pi-\pi$ interactions, respectively) in **5**.

regular (the grid looks like a square), while those of **3** and **4** are distorted as rhombus. Because the bridging distance of the bending dicarboxylate $nipa^{2-}$ is shorter than that of bdc^{2-}, the grid size of **5** is smaller than those of **3** and **4**. The different shapes of the 2D layers result in different packing modes. In **5**, two layers interdigitate by the $nipa^{2-}$ side to form a double-layer structure, leaving the bphy ligands in the outside of the double layer (Figure 3c). The closest contact between the two layers is the very strong $\pi-\pi$ interaction between the nitrobenzene moiety of $nipa^{2-}$ (3.4 Å). These double layers further stack to form the 3D structure via N−H···O hydrogen bonding between the hydrazo and carboxylate groups [N···O 2.851(3)−2.862(1) Å; N−H···O 152.3(1)−171.2(3)°] and the $\pi-\pi$-stacking interactions between the pyridyl rings of the bphy ligands (Figures S7 and S8 in the Supporting Information). Compared to the structures of **3** and **4**, the staggered stacking mode of **5** is more similar to those of common 2D structures. Owing to the quite small lattice size, **5** possesses a small solvent-accessible void of 21.6%. Because all of the hydrazo groups are employed to form interlayer hydrogen bonds, there is no strong hydrogen bond [C···O 3.558(7) Å] between the guest molecules and the framework.

In **6**, there are one Co^{2+}, half of a bdc^{2-} ligand, one bphy, and one Br^- in the asymmetric unit. The Co^{2+} ion is coordinated by a monodentate carboxylate [Co−O 1.971(4) Å] and two pyridyl groups [Co−N 2.020(5)−2.025(5) Å] from two bphy ligands and a Br^- ion [Co−Br 2.396(1) Å] to furnish a distorted tetrahedral geometry (Figure 4a). These Co^{2+} ions are

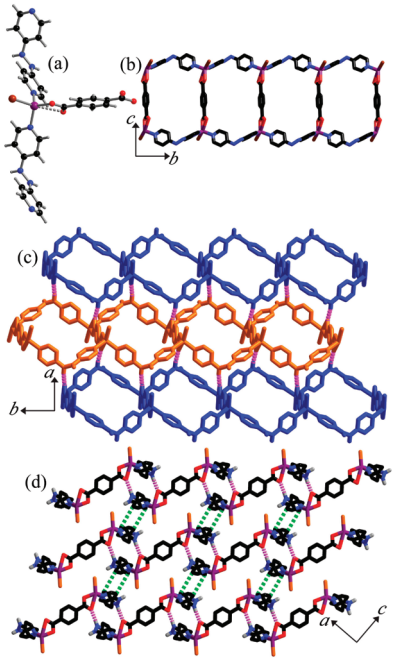

Figure 4. Perspective views of (a) the coordination environment of the Co atom, (b) the ladderlike 1D coordination network, (c) the hydrogen-bonding interaction of the ladder, and (d) the 3D supramolecular structure sustained by hydrogen-bonding (pink dotted lines) and $\pi-\pi$-stacking (green dotted lines) interactions in **6**.

connected by bidentate bphy ligands to form a 1D wavy chain. Two chains as side pieces are bridged together by ditopic bdc^{2-} ligands as rungs into a molecular ladder (Figure 4b). The adjacent Co···Co separations bridged by the bphy and bdc^{2-} ligands are 10.75 and 10.95 Å, respectively. Each ladder forms strong hydrogen bonds with two neighbors using the hydrazo and carboxylate groups [N···O 2.795(7) Å; N−H···O 171.5(2)°], giving a 2D hydrogen-bonding-layered structure (Figure 4c). Adjacent layers are then packed via $\pi-\pi$-stacking interactions to form a 3D supramolecular architecture (Figures 4d and S2 and S4 in the Supporting Information). By virtue of

dx.doi.org/10.1021/ic300097y | Inorg. Chem. 2012, 51, 5686−5692

the directional hydrogen-bonding and $\pi-\pi$-stacking interactions, the ladders do not interdigitate with each other. Consequently, the whole framework possesses a large solvent-accessible void of 45.9%, in which the guest DMA molecules are anchored to the host framework by hydrogen bonds with the hydrazo groups [N···O 2.735(4) Å; N−H···O 169.7(5)°].

Framework Stability. Thermogravimetric (TG) curves show that **3**−**6** release all of the guests at 190, 180, 150, and 240 °C and decompose at 300, 370, 390, and 350 °C, respectively. Their amounts of released guests match well with their formulas (see the Supporting Information).

VTPXRD patterns show that **3** and **4** can be converted to new phases after guest removal, indicating flexibility of these frameworks (Figures S11 and S14 in the Supporting Information). Because **1a**/**1b**/**1** and **3** have the same framework composition but different topologies, we have checked whether a structural transformation between **1a**/**1b**/**1** and **3** takes place upon removal of the solvents. We have demonstrated that **1a** and **1b** could convert to the same phase **1** after their guests are removed.[31] However, the PXRD patterns of **1a**, **1b**, **1**, **3**, and guest-free **3** are different with each other (Figure S11 in the Supporting Information). In other words, a structural transformation between **1a**/**1b**/**1** and **3** would not take place. The PXRD pattern of the guest-free sample of **5** matches well with its as-synthesized phase, suggesting that its framework is rigid, probably related to its relatively close-packing structure (Figures S17 and S19 in the Supporting Information). For **6**, the PXRD pattern of its guest-free sample became weaker and broader, indicating that the host framework lost long-range order or collapsed partially (Figure S20 in the Supporting Information). In order to verify the reversibility in the structure conversions of **3**, **4**, and **6**, their activated samples were exposed in DMF and/or DMA vapors. After several hours, PXRD patterns show that the activated samples of **3** and **4** transform back to their as-synthesized structures. However, guest-free **6** can hardly be recovered to the good crystallinity of the as-synthesized **6** even after several weeks.

Sorption Studies. Gas sorption studies were carried out to evaluate the porosity of guest-free **3**, **4**, and **6** because their crystal structures contain relatively large solvent-accessible voids. The activation conditions were optimized based on the above-mentioned TG and VTPXRD results. The as-synthesized samples of **3**, **4**, and **6** were heated at different temperatures under high vacuum for about 8 h and then further checked by PXRD and TG measurements to confirm the complete removal of template molecules and retention of high crystallinity. The results indicated that the activation temperatures of **3** and **4** should be 190 and 180 °C, as indicated by TG analyses, while the framework of **6** could be activated at 200 °C. The CO_2 sorption isotherms of **3**, **4**, and **6** measured at 195 K showed type I isotherm characteristics, illustrating the microporous nature of these samples (Figure 5). The CO_2-saturated uptakes of **3** and **6**, only 24 and 35 $cm^3\ g^{-1}$, respectively, are significantly lower than the theoretical values estimated from the crystal structures (262 and 301 $cm^3\ g^{-1}$). Besides, the isotherms of **3** and **6** represent obvious hysteresis, illustrating that there is a great barrier for the gas diffusion. All of these phenomena indicate that the structures of **3** and **6** severely are deformed into relatively condensed phases after guest removal, which can accommodate relatively small amounts of gas molecules and also hamper the gas diffusion. In contrast, **4** exhibits a relatively high saturated adsorption at 195 K (131 $cm^3\ g^{-1}$), corresponding to a pore volume of 0.15 $cm^3\ g^{-1}$,

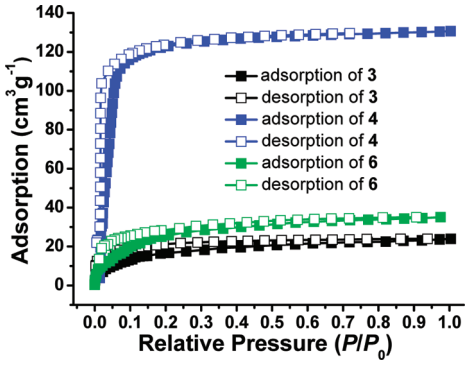

Figure 5. CO_2 isotherms measured at 195 K.

although it is only one-third of the calculated amount (0.44 $cm^3\ g^{-1}$) from its single-crystal structure. As mentioned above, the structure of **4** also undergoes phase transition after guest removal, just similar to that of **3**. Compared to guest-free **3**, guest-free **4** can be obviously opened by CO_2 at 195 K. Moreover, the isotherm for guest-free **4** is very steep at low pressure. The onset pressure is very low (if any), and there is only very small hysteresis, implying that the framework of guest-free **4** is very flexible and can be opened by CO_2 at very low pressure. Of course, the onset pressure of adsorption should be changed along with the temperature and/or guests. For example, we have demonstrated that **2**, showing flexible behavior similar to that of **4**, could be used to efficiently separate CO_2 and CH_4. At 298 K, guest-free **2** started to adsorb in a little CO_2 and totally opened its pore at about 22 bar, while it could hardly adsorb in CH_4 up to 40 bar. In short, considering the lower onset pressure and the more dramatic step of the CO_2 isotherm, **4** may exhibit a better CO_2/CH_4 separation performance.

CO_2 and CH_4 sorption isotherms were measured for **4** at 298 K with pressure up to 40 bar (Figure 6a). The CO_2 uptake is very low below 5 bar (3.8 $cm^3\ g^{-1}$). After that, the uptake suddenly increases to 81 $cm^3\ g^{-1}$ at 6 bar and further increases to 147 $cm^3\ g^{-1}$ at 40 bar gradually. Although at 298 K and 40 bar the pressure is far away from the saturated vapor pressure 64 bar ($P/P_0 = 0.6$), the adsorption amount is obviously higher than that of $P/P_0 = 1$ at 195 K, suggesting that the increasing temperature is beneficial to increasing framework flexibility, which has been observed in other PCPs.[34−37] In contrast, almost no CH_4 could be adsorbed up to 40 bar (2.0 $cm^3\ g^{-1}$). Consequently, the CO_2/CH_4 uptake ratio changes basically according to the CO_2 isotherm shape (Figure 6b). Between 0 and 5 bar, the CO_2/CH_4 uptake ratio gradually increases from 2 to 36 and then sharply increases to a maximum of 466 at 6 bar. Although the ratio gradually decreases at higher pressures, it is still 75 at 40 bar. For comparison, we also calculated the pressure-dependent CO_2/CH_4 uptake ratio for **2**, which has a shape similar to that for **4** because the two frameworks both undergo a gate-opening process during CO_2 adsorption. However, the maximum CO_2/CH_4 uptake ratio for **2** is only 22, which locates at a relatively high pressure of 22 bar. The adsorption isotherms of the strong adsorbate CO_2 reveal the different framework flexibility and the location of the maximum CO_2/CH_4 uptake ratios of **2** and **4**. The host framework of **2** can be completely opened, but the phase transition occurs gradually between 10 and 22 bar. In contrast, the host framework of **4** can be only opened to one-third of the as-synthesized phase, but its phase transition occurs suddenly

dx.doi.org/10.1021/ic300097y | Inorg. Chem. 2012, 51, 5686−5692

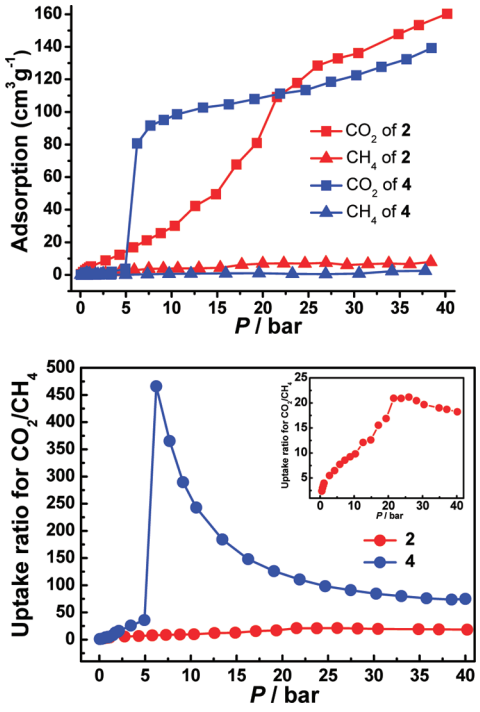

Figure 6. High-pressure CO_2 and CH_4 (a) adsorption isotherms and (b) CO_2/CH_4 uptake ratios of **2** and **4** measured at 298 K (inset: magnified CO_2/CH_4 uptake ratios of **4**).

between 5 and 6 bar. For adsorbents based on exclusion mechanisms such as the size selectivity and gate opening, the uptake of weaker adsorbate is most important in determining the adsorption selectivity. The guest-free phase of **2** contains more accessible pores than those of **4**, although they both can be described as nonporous. Therefore, **2** can adsorb more CH_4 than **4** in the whole measured pressure region, which significantly reduces the CO_2/CH_4 selectivity of **2**. In summary, because of the different framework flexibility from **2**, **4** can separate CO_2/CH_4 more efficiently because of not only the high adsorption ratios but also the higher ratio appearing at lower pressure, which is beneficial for energy savings. This interpretation may also be suitable for understanding why guest-free **3** cannot show gated sorption behavior. Although the frameworks of **2**−**4** all show structural flexibility upon removal of solvent/template molecules (high boiling points and ability to strongly interact with the frameworks), the different thermodynamic characteristics, i.e., energy difference or energy barrier between multiple thermodynamically stable states, can be revealed by the gas molecules CO_2/CH_4 (low boiling points and ability to weakly interact with the frameworks).

CONCLUSIONS

In summary, four new low-dimensional coordination polymers with similar coordination structures have been synthesized by adopting a new solvothermal in situ ligand reaction with different secondary ligands and reaction conditions. The solvothermal in situ reduction of azpy to bphy is further proven to be an effective strategy for the crystal engineering of coordination polymers. As observed in the diverse interpenetration/packing structures and supramolecular interactions of these low-dimensional coordination frameworks, bphy represents a unique ligand for the construction of flexible coordination networks. More importantly, the framework flexibility plays an important role in determining the gas separation performance. Although rational design and control of the framework structure and flexibility is still of great challenge, systematic structure modulation of highly similar coordination framework structures could serve as a viable way for the discovery of excellent gas separation materials.

ASSOCIATED CONTENT

Supporting Information

Additional plots, TG analyses, and PXRD patterns, as well as X-ray data files in CIF format. This material is available free of charge via the Internet at http://pubs.acs.org.

AUTHOR INFORMATION

Corresponding Author

*E-mail: zhangjp7@mail.sysu.edu.cn (J.-P.Z.), cxm@mail.sysu.edu.cn (X.-M.C.).

Notes

The authors declare no competing financial interest.

ACKNOWLEDGMENTS

This work was supported by the "973 Project" (Grant 2012CB821706), NSFC (Grants 21121061 and 21001120), and Chinese Ministry of Education (Grants NCET-10-0863 & ROCS).

REFERENCES

(1) Xie, Z. G.; Ma, L. Q.; deKrafft, K. E.; Jin, A.; Lin, W. B. *J. Am. Chem. Soc.* **2010**, *132*, 922.
(2) Xie, Y. M.; Yu, R. M.; Wu, X. Y.; Wang, F.; Chen, S. C.; Lu, C. Z. *CrystEngComm* **2010**, *12*, 3490.
(3) Chu, Q.; Su, Z.; Fan, J.; Okamura, T.; Lv, G. C.; Liu, G. X.; Sun, W. Y.; Ueyama, N. *Cryst. Growth Des.* **2011**, *11*, 3885.
(4) Zhang, X. M.; Hao, Z. M.; Zhang, W. X.; Chen, X. M. *Angew. Chem., Int. Ed.* **2007**, *46*, 3456.
(5) Zhou, X.-P.; Li, M.; Liu, J.; Li, D. *J. Am. Chem. Soc.* **2011**, *134*, 67.
(6) Alkordi, M. H.; Belof, J. L.; Rivera, E.; Wojtas, L.; Eddaoudi, M. *Chem. Sci.* **2011**, *2*, 1695.
(7) Ohtani, R.; Yoneda, K.; Furukawa, S.; Horike, N.; Kitagawa, S.; Gaspar, A. B.; Munoz, M. C.; Real, J. A.; Ohba, M. *J. Am. Chem. Soc.* **2011**, *133*, 8600.
(8) Yuan, D. Q.; Lu, W. G.; Zhao, D.; Zhou, H. C. *Adv. Mater.* **2011**, *23*, 3723.
(9) Wu, S. T.; Ma, L. Q.; Long, L. S.; Zheng, L. S.; Lin, W. B. *Inorg. Chem.* **2009**, *48*, 2436.
(10) Chang, Z.; Zhang, D. S.; Chen, Q.; Li, R. F.; Hu, T. L.; Bu, X. H. *Inorg. Chem.* **2011**, *50*, 7555.
(11) Zeng, M. H.; Wang, Q. X.; Tan, Y. X.; Hu, S.; Zhao, H. X.; Long, L. S.; Kurmoo, M. *J. Am. Chem. Soc.* **2010**, *132*, 2561.
(12) Takashima, Y.; Martinez, V. M.; Furukawa, S.; Kondo, M.; Shimomura, S.; Uehara, H.; Nakahama, M.; Sugimoto, K.; Kitagawa, S. *Nat. Commun.* **2011**, *2*, 168.
(13) Seeber, G.; Cooper, G. J. T.; Newton, G. N.; Rosnes, M. H.; Long, D. L.; Kariuki, B. M.; Kogerler, P.; Cronin, L. *Chem. Sci.* **2010**, *1*, 62.
(14) Kitagawa, S.; Kitaura, R.; Noro, S. *Angew. Chem., Int. Ed.* **2004**, *43*, 2334.
(15) Kitagawa, S.; Uemura, K. *Chem. Soc. Rev.* **2005**, *34*, 109.
(16) Zhang, J. P.; Qi, X. L.; He, C. T.; Wang, Y.; Chen, X. M. *Chem. Commun.* **2011**, *47*, 4156.
(17) Wang, C. C.; Yang, C. C.; Yeh, C. T.; Cheng, K. Y.; Chang, P. C.; Ho, M. L.; Lee, G. H.; Shih, W. J.; Sheu, H. S. *Inorg. Chem.* **2011**, *50*, 597.
(18) Chen, D.; Liu, Y. J.; Lin, Y. Y.; Zhang, J. P.; Chen, X. M. *CrystEngComm* **2011**, *13*, 3827.

(19) Kondo, A.; Nakagawa, T.; Kajiro, H.; Chinen, A.; Hattori, Y.; Okino, F.; Ohba, T.; Kaneko, K.; Kanoh, H. *Inorg. Chem.* **2010**, *49*, 9247.
(20) Arslan, H. K.; Shekhah, O.; Wieland, D. C. F.; Paulus, M.; Sternemann, C.; Schroer, M. A.; Tiemeyer, S.; Tolan, M.; Fischer, R. A.; Woll, C. *J. Am. Chem. Soc.* **2011**, *133*, 8158.
(21) Inubushi, Y.; Horike, S.; Fukushima, T.; Akiyama, G.; Matsuda, R.; Kitagawa, S. *Chem. Commun.* **2010**, *46*, 9229.
(22) Xiang, S. C.; Zhang, Z. J.; Zhao, C. G.; Hong, K. L.; Zhao, X. B.; Ding, D. R.; Xie, M. H.; Wu, C. D.; Das, M. C.; Gill, R.; Thomas, K. M.; Chen, B. L. *Nat. Commun.* **2011**, *2*, 204.
(23) Demessence, A.; Long, J. R. *Chem.—Eur. J.* **2010**, *16*, 5902.
(24) Jin, Z.; Zhao, H. Y.; Zhao, X. J.; Fang, Q. R.; Long, J. R.; Zhu, G. S. *Chem. Commun.* **2010**, *46*, 8612.
(25) Uemura, T.; Yanai, N.; Watanabe, S.; Tanaka, H.; Numaguchi, R.; Miyahara, M. T.; Ohta, Y.; Nagaoka, M.; Kitagawa, S. *Nat. Commun.* **2010**, *1*, 83.
(26) Colombo, V.; Galli, S.; Choi, H. J.; Han, G. D.; Maspero, A.; Palmisano, G.; Masciocchi, N.; Long, J. R. *Chem. Sci.* **2011**, *2*, 1311.
(27) Cheng, Y.; Kajiro, H.; Noguchi, H.; Kondo, A.; Ohba, T.; Hattori, Y.; Kaneko, K.; Kanoh, H. *Langmuir* **2011**, *27*, 6905.
(28) Ma, S.; Sun, D.; Wang, X.-S.; Zhou, H.-C. *Angew. Chem., Int. Ed.* **2007**, *46*, 2458.
(29) He, Y. B.; Xiang, S. C.; Chen, B. L. *J. Am. Chem. Soc.* **2011**, *133*, 14570.
(30) Kanoo, P.; Mostafa, G.; Matsuda, R.; Kitagawa, S.; Maji, T. K. *Chem. Commun.* **2011**, *47*, 8106.
(31) Liu, X. M.; Xie, L. H.; Lin, J. B.; Lin, R. B.; Zhang, J. P.; Chen, X. M. *Dalton Trans.* **2011**, *40*, 8549.
(32) Launay, J. P.; Tourrel-Pagis, M.; Lipskier, J. F.; Marvaud, V.; Joachim, C. *Inorg. Chem.* **1991**, *30*, 1033.
(33) Spek, A. L. *J. Appl. Crystallogr.* **2003**, *36*, 7.
(34) Choi, H. J.; Dinca, M.; Long, J. R. *J. Am. Chem. Soc.* **2008**, *130*, 7848.
(35) Walton, K. S.; Millward, A. R.; Dubbeldam, D.; Frost, H.; Low, J. J.; Yaghi, O. M.; Snurr, R. Q. *J. Am. Chem. Soc.* **2008**, *130*, 406.
(36) Zhang, J. M.; Wu, H. H.; Emge, T. J.; Li, J. *Chem. Commun.* **2010**, *46*, 9152.
(37) Matsuda, R.; Tsujino, T.; Sato, H.; Kubota, Y.; Morishige, K.; Takata, M.; Kitagawa, S. *Chem. Sci.* **2010**, *1*, 315.